

# InAs/InAsSb Type-II Superlattice Mid-Wavelength Infrared Focal Plane Array With Significantly Higher Operating Temperature Than InSb

Volume 10, Number 6, December 2018

David Z. Ting, *Senior Member, IEEE*

Sir B. Rafol

Sam A. Keo, *Member, IEEE*

Jean Nguyen

Arezou Khoshakhlagh

Alexander Soibel

Linda Höglund, *Member, IEEE*

Anita M. Fisher

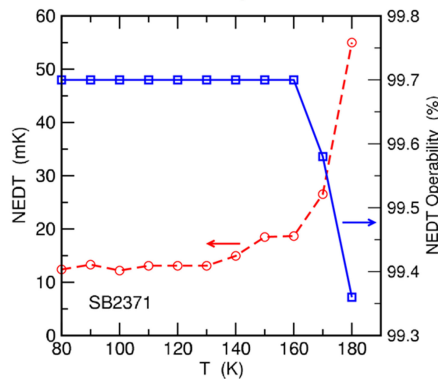
Edward M. Luong

Jason M. Mumolo

John K. Liu

Sarath D. Gunapala, *Fellow, IEEE*


InAs/InAsSb Type-II Superlattice High Operating Temperature Mid-Wavelength Infrared Focal Plane Array



DOI: 10.1109/JPHOT.2018.2877632

1943-0655 © 2018 IEEE

# InAs/InAsSb Type-II Superlattice Mid-Wavelength Infrared Focal Plane Array With Significantly Higher Operating Temperature Than InSb

David Z. Ting , *Senior Member, IEEE*, Sir B. Rafol, Sam A. Keo, *Member, IEEE*, Jean Nguyen, Arezou Khoshakhlagh, Alexander Soibel, Linda Höglund, *Member, IEEE*, Anita M. Fisher, Edward M. Luong, Jason M. Mumolo, John K. Liu, and Sarath D. Gunapala, *Fellow, IEEE*

NASA Jet Propulsion Laboratory, California Institute of Technology, Pasadena, CA 91109 USA

DOI:10.1109/JPHOT.2018.2877632  
U.S. Government work not protected by U.S. copyright.

Manuscript received September 5, 2018; revised October 13, 2018; accepted October 17, 2018. Date of current version November 13, 2018. The work was carried out at the Jet Propulsion Laboratory, California Institute of Technology, under a contract with the National Aeronautics and Space Administration. Government sponsorship acknowledged. Corresponding author: David Z. Ting (e-mail: david.z.ting@jpl.nasa.gov).

**Abstract:** We report focal plane array (FPA) results on a mid-wavelength InAs/InAsSb type-II strained layer superlattice (T2SLS) unipolar barrier infrared detector with a cutoff wavelength of 5.4  $\mu\text{m}$ . For 300 K background in the 3–5- $\mu\text{m}$  band,  $f/2$  aperture, an FPA operating at 150 K exhibits a mean noise equivalent differential temperature (NEDT) of 18.5 mK, and an NEDT operability of 99.7%. The  $\text{NE}\Delta T$  distribution has a width of 8 mK, with no noticeable distribution tail, indicating excellent uniformity. The mean noise-equivalent irradiance is  $9.1 \times 10^{11}$  photons/sec- $\text{cm}^2$ . The mean quantum efficiency is 49.1% without antireflection coating, and the mean specific detectivity ( $D^*$ ) is  $2.53 \times 10^{11}$   $\text{cm}\cdot\text{Hz}^{1/2}/\text{W}$ . Benefitting from an absorber material with a much longer Shockley–Read–Hall minority carrier lifetime, and a device architecture that suppresses generation-recombination and surface-leakage dark current, the InAs/InAsSb T2SLS barrier infrared detector FPA has demonstrated a significantly higher operating temperature than the mid-wavelength infrared market-leading InSb.

**Index Terms:** Infrared detector, photodetector, type-II superlattice, InAs/InAsSb, heterostructure, unipolar barrier, nBn, focal plane array.

## 1. Introduction

InSb is one of the most widely used infrared photodetector material. It is a robust III-V semiconductor with favorable focal plane array (FPA) manufacturability, and its band gap is ideally suited for covering the 3–5  $\mu\text{m}$  mid-wavelength infrared (MWIR) atmospheric transmission window. The InSb FPA offers high operability, high uniformity, large-format capability, and affordability, and has been dominating the MWIR FPA market in volume. Despite its success, InSb has notable drawbacks compared to HgCdTe (MCT), the major competing MWIR FPA technology based on II-VI semiconductors. The Shockley-Read-Hall (SRH) lifetime for InSb is  $\sim 400$  ns, which is short compared to that of the MWIR MCT [1]. Unlike MCT which can be passivated effectively using the high band gap CdTe, InSb lacks heterostructure capability, and achieving good surface passivation is more challenging. As a result

the InSb FPA operates at much lower temperatures ( $\sim 80$  K for ion-implant planar InSb; 95–100 K for MBE grown epi-InSb) than the MWIR MCT FPA [2], [3]. Another disadvantage of InSb is that, unlike MCT, which provides a continuously adjustable cutoff wavelength ranging from the near infrared (NIR) to very long wavelength infrared (VLWIR), InSb has a fixed cutoff wavelength at  $\sim 5.3 \mu\text{m}$ . Recent advances in infrared detector material and device architecture have made it possible to improve III-V MWIR detectors. The unipolar barrier device architecture such as the nBn [4], [5], the XBn [6], [7], the pMp [8], and the complementary barrier infrared detector (CBIRD) [9], [10] can be used to reduce generation-recombination (G-R) dark current due to SRH processes, as well as to suppress surface leakage dark current [4], [11], [12]. The initial nBn devices were implemented using either InAs absorber grown on InAs substrate, or lattice-matched  $\text{InAs}_{0.91}\text{Sb}_{0.09}$  grown on GaSb substrate, with cutoff wavelengths of  $\sim 3.2 \mu\text{m}$  and  $\sim 4 \mu\text{m}$ , respectively. While they have good detector performance, they do not provide full coverage of the MWIR transmission window. Cutoff wavelength extension to longer than  $5 \mu\text{m}$  can be achieved easily by using the InAs/GaSb type-II superlattice (T2SL), which also has the advantage of being readily amenable to the unipolar device architecture [13]–[15]. However, the minority carrier lifetime of the MWIR InAs/GaSb T2SL at 80 ns [16] is significantly shorter than that of InSb. On the other hand, the more recently emerged InAs/InAsSb type-II strained layer superlattice (T2SLS), has demonstrated longer minority carrier lifetimes than the InAs/GaSb T2SL [17]. In particular, the MWIR InAs/InAsSb T2SLS has exhibited SRH lifetimes of  $\sim 10 \mu\text{s}$  [18], [19], which is much longer than the typical InSb SRH lifetime of 400 ns [1]. In this paper, we report results on an InAs/InAsSb T2SLS unipolar barrier infrared detector based MWIR FPA, which exhibits significantly higher operating temperature than InSb FPAs.

## 2. InAs/InAsSb Type-II Superlattice High Operating Temperature (Hot) Barrier Infrared Detector (Bird)

We described in a patent disclosure [20] the general concept of building unipolar barrier infrared detectors using absorbers based on superlattices where each period contains at least an InAsSb layer, and at least one other layer selected from InAs, InGaAs, and InAsSb; in particular, this includes the InAs/InAsSb superlattice. Compared to the more established InAs/GaSb T2SL, the InAs/InAsSb T2SLS is an alternative with simpler growth [20], better defect tolerance, longer minority lifetimes [17]–[19], but smaller cutoff wavelength range. At longer cutoff wavelengths, the InAs/InAsSb T2SLS also has weaker optical absorption [21], [22], and more challenging vertical hole transport [23], [24]. For MWIR, the InAs/InAsSb T2SLS properties are overall more favorable. We have recently reported detailed experimental results on a mid-wavelength (MW) InAs/InAsSb T2SLS high operating temperature (HOT) barrier infrared detector (BIRD) [25]; we provided a brief summary of the discrete detector results in this section.

We designed and fabricated an nBn device using an InAs/InAsSb T2SL absorber and an AlAsSb electron unipolar barrier, with a cutoff wavelength exceeding  $5 \mu\text{m}$ . The detector structure consists of a  $\sim 670 \text{ \AA}$  top contact layer, a  $1,200 \text{ \AA}$  electron unipolar barrier layer, and a  $\sim 2.6 \mu\text{m}$  thick absorber layer grown on 3-inch GaSb substrate by molecular beam epitaxy. Both the top contact and absorber layers consist of not-intentionally-doped ( $37 \text{ \AA}$ ,  $13 \text{ \AA}$ )-InAs/InAs<sub>0.66</sub>Sb<sub>0.34</sub> superlattice, and the barrier material is  $1 \times 10^{15} \text{ cm}^{-3}$  Be doped AlAs<sub>0.085</sub>Sb<sub>0.915</sub>. The nBn detector wafer (Sample Sb-2371) is processed into discrete detectors and focal plane arrays (FPAs) for characterization.

Fig. 1(a) shows the dark current density – voltage characteristics of a  $250 \mu\text{m} \times 250 \mu\text{m}$  square mesa photodiode taken at 147 K. The dark current density at  $-0.2 \text{ V}$  is  $3 \times 10^{-5} \text{ A/cm}^2$ , which is approximate 6 times that given by the MCT Rule 07 [26]. Fig. 1(b) shows back-side illuminated spectral quantum efficiency (QE) for the device without anti-reflection coating, taken under  $-0.2 \text{ V}$  bias at 150 K. The cutoff, taken as the wavelength at which the QE is 1/2 of that at  $\lambda = 4.5 \mu\text{m}$  ( $\sim 52\%$  in this case), is  $\sim 5.37 \mu\text{m}$ . The surface reflectivity is  $\sim 1/3$ , and the estimated absorption coefficient is  $\sim 2,200 \text{ cm}^{-1}$ . Fig. 2(a) shows an Arrhenius plot of the temperature dependence of dark current density under  $-0.2 \text{ V}$  bias. A fit over the 109 K to 222 K range to the expression

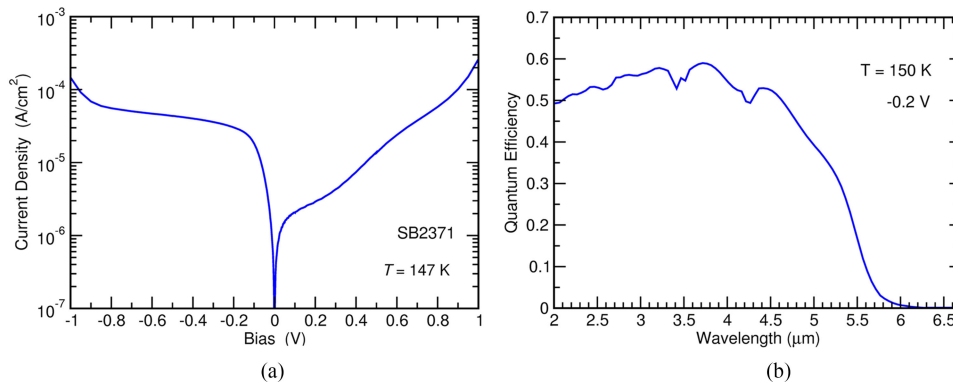


Fig. 1. (a) MWIR InAs/InAsSb T2SLS nBn detector Sb-2371 dark current density vs. applied bias at 147 K. (b) 150 K spectral quantum efficiency (QE) for Sb-2371, without anti-reflection coating.

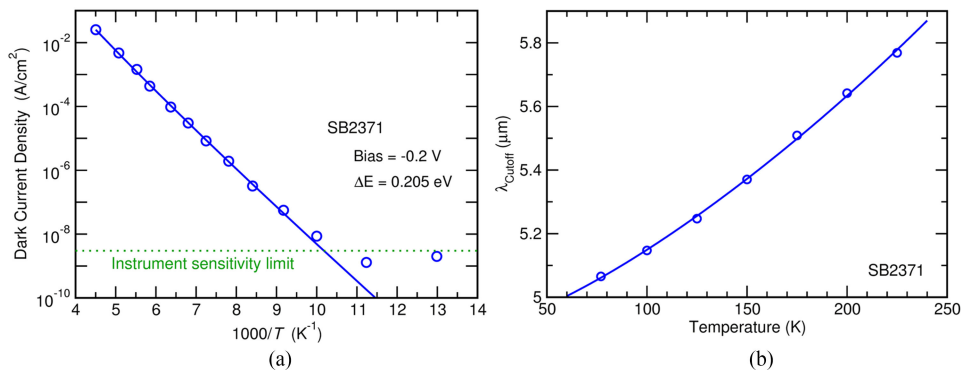


Fig. 2. (a) The temperature dependence of Sb-2371 dark current density at  $-0.2$  V bias. (b) The cutoff wavelength of Sb-2371 as a function of temperature.

$CT^3 \exp(-\Delta E/k_B T)$  yields an activation energy of  $\Delta E = 0.205$  eV, which is fairly close to the band gap ( $\sim 0.230$  eV at 150 K). The Arrhenius analysis indicates near diffusion-limited dark current behavior down to  $\sim 100$ -K (below which we reached our dark current measurement instrument sensitivity limit). Fig. 2(b) shows the cutoff wavelength temperature dependence. Like InSb (and unlike MCT), the cutoff wavelength increases with rising operating temperature. Taking the band gap temperature dependence from the cutoff wavelength, and fitting to the Varshni expression  $E_g(T) = E_{g0} - AT^2/(B + T)$ , we find  $E_{g0} = 0.2537$  eV,  $A = 2.404 \times 10^{-4}$  eV/K, and  $B = 85.85$  K. More details of the single-element detector results can be found in Ref. [25].

### 3. Hot-Bird Focal Plane Array

We have fabricated FPAs using the HOT-BIRD material Sb-2371. The detector pixels are defined by a dry etch process, with an etch depth of  $\sim 3,000$  Å into the absorber layer. The detector array is hybridized to the  $24\text{-}\mu\text{m}$  pitch,  $640 \times 512$  format SBF-193 direction injection (DI) readout integrated circuit (ROIC), which has a well capacity of 8 million electrons. The GaSb substrate is completely removed after epoxy under-filling. The FPA 12GAL11 is characterized under 300 K background illumination and  $f/2$  aperture. The cutoff wavelength at  $T = 150$  K is  $\sim 5.4$   $\mu\text{m}$ . Fig. 3(a) and (b) respectively show the noise equivalent differential temperature ( $NE\Delta T$ ) operability and the mean  $NE\Delta T$  as functions of FPA operating temperature. The  $NE\Delta T$  operability is 99.7% at up to 160 K, and decreases to 99.3% at 180 K. The mean  $NE\Delta T$  is below 19 mK for temperatures up to 160 K, and increases to  $\sim 55$  mK at 180 K. Fig. 4(a) and (b) respectively show the  $NE\Delta T$  and NEI (noise-

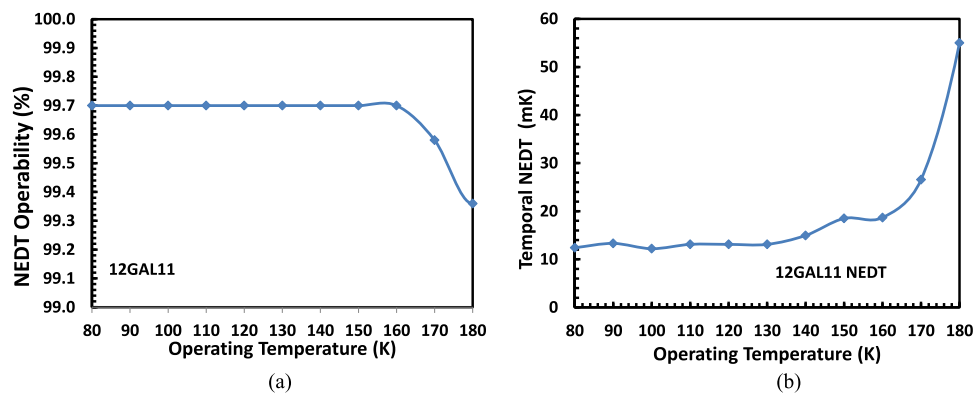


Fig. 3. (a) NEDT operability and (b) mean NEDT as functions of FPA operating temperature.

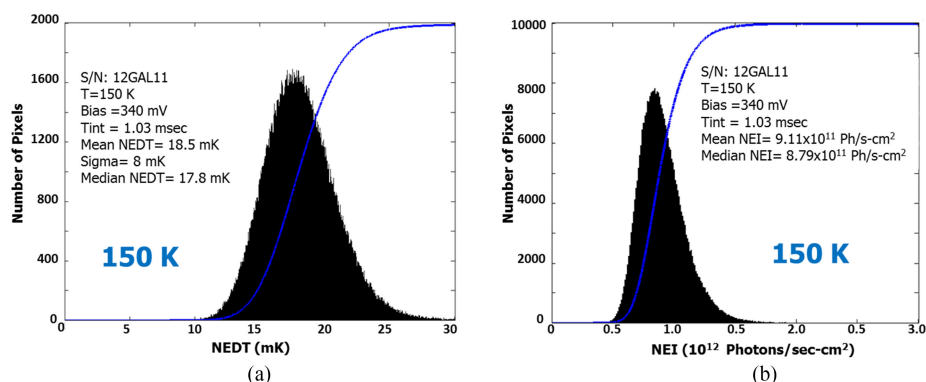


Fig. 4. NE $\Delta$ T and NEI histograms for a  $640 \times 512$  format HOT-BIRD FPA operating at  $T = 150$  K, measured with  $f/2$  optics at  $300$  K background in the  $3\text{--}5 \mu\text{m}$  band. The cumulative distributions are indicated by the blue curves.

equivalent irradiance) distributions taken at an FPA temperature of  $150$  K. The average NE $\Delta$ T at  $T = 150$  K is  $18.5$  mK, and the average NEI is  $9.1 \times 10^{11}$  photons/sec-cm<sup>2</sup>. The NE $\Delta$ T distribution has a width of  $8$  mK, with no noticeable distribution tail, indicating excellent uniformity.

Fig. 5 shows the  $150$  K external QE and specific detectivity ( $D^*$ ) histograms. The mean QE (no anti-reflection coating) is  $49.1\%$ , and the mean  $D^*$  is  $2.53 \times 10^{11}$  cm-Hz<sup>1/2</sup>/W. The QE distribution was not corrected for the  $\cos^4$  effect. The  $3\sigma$  integrated blackbody detectivity operability is  $99.9\%$  at  $150$  K. Fig. 6 shows two-point corrected images taken with the FPA at  $T = 150, 160, 170,$  and  $180$  K. Overall, we find that it is relatively straight-forward to fabrication HOT-BIRD FPAs with high uniformity and good temperature performance.

#### 4. Discussions and Summary

Currently the two main mid-wavelength infrared focal plane array technologies are based on InSb and HgCdTe infrared absorbers, each with its own distinct advantages. InSb dominates the MWIR FPA market in volume because of the superior manufacturability afforded by the robustness of III-V semiconductors. On the other hand, the II-VI semiconductor based MCT can achieve much lower dark current and higher operating temperature, and is the detector of choice for more demanding applications. In this paper, we report FPA results on a mid-wavelength InAs/InAsSb type-II strained layer superlattice high operating temperature (HOT) unipolar barrier infrared detector (BIRD) that essentially combines the advantages of III-V semiconductor robustness and MCT high performance.

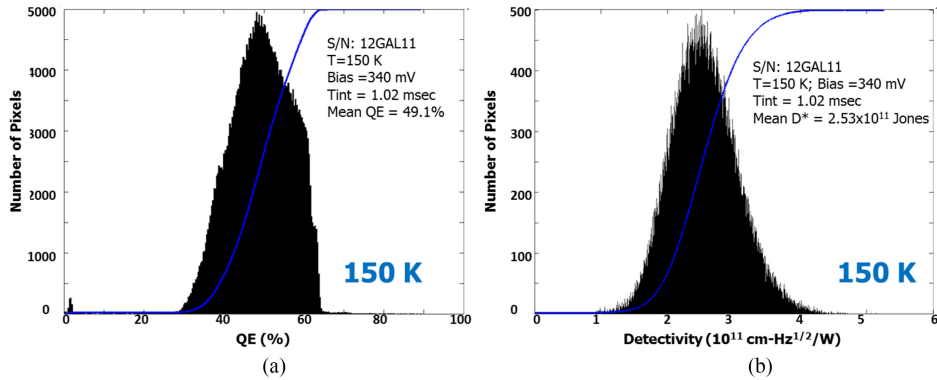


Fig. 5. Quantum efficiency (QE) and specific detectivity ( $D^*$ ) histograms for a  $640 \times 512$  format HOT-BIRD FPA operating at  $T = 150$  K, measured with  $f/2$  aperture at 300 K background in the 3–5  $\mu\text{m}$  band. The cumulative distributions are indicated by the blue curves.

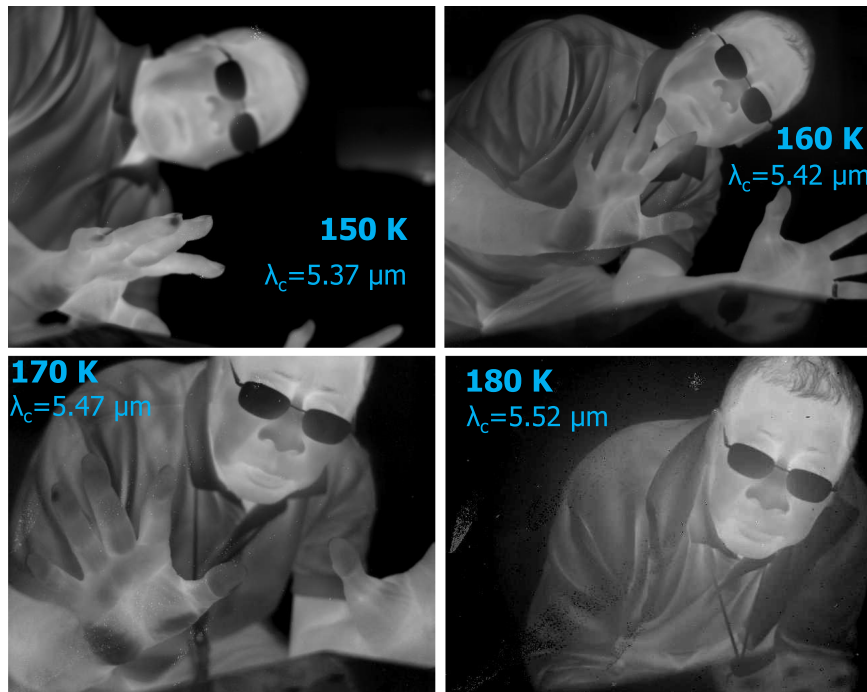


Fig. 6. Images taken at  $T = 150, 160, 170$  and  $180$  K, for a  $640 \times 512$  format FPA (12GAL11).

A 24- $\mu\text{m}$  pitch,  $640 \times 512$  format FPA with a cutoff wavelength of  $\sim 5.4 \mu\text{m}$  exhibits a 300 K background,  $f/2$  aperture mean NEDT of 18.5 mK, and an NEDT operability of 99.7% at 150 K. The  $\text{NE}\Delta T$  distribution has a width of 8 mK, with no noticeable distribution tail, indicating excellent uniformity. The InAs/InAsSb T2SLS FPA has the same cutoff wavelength as InSb, but can work at much higher operating temperature to provide reduced cryocooler size, weight, and power consumption requirements. The higher operating temperature advantage of the InAs/InAsSb T2SLS barrier infrared detector over InSb results from (1) longer absorber material SRH minority carrier lifetime, and, (2) the unipolar device architecture providing generation-recombination and surface-leakage dark current suppression. While InSb has a fixed cutoff wavelength, InAs/InAsSb T2SLS

also offers continuous cutoff wavelength adjustability ranging from the mid-wavelength infrared to the very long wavelength infrared, providing greater versatility.

## Acknowledgment

The authors would like to thank S. Bandara, R. E. DeWames, D. R. Rhiger, W. E. Tennant, and J. N. Schulman for their helpful discussions, and C. J. Hill and R. S. Kowalczyk for their technical assistance.

## References

- [1] M. A. Kinch, *State-of-the-Art Infrared Detector Technology*. Bellingham, WA, USA: SPIE, 2014. doi: [10.1117/3.1002766](https://doi.org/10.1117/3.1002766).
- [2] M. Vuillermet *et al.*, "HOT infrared detectors using MCT technology," in *Proc. SPIE Infrared Technol. Appl.*, May 2011, vol. 8012, Art. no. 80122W. doi: [10.1117/12.885601](https://doi.org/10.1117/12.885601).
- [3] P. Klipstein *et al.*, "Recent progress in InSb based quantum detectors in Israel," *Infrared Phys. Technol.*, vol. 59, pp. 172–181, 2013. [Online]. Available: <https://doi.org/10.1016/j.infrared.2012.12.035>
- [4] S. Maimon and G. W. Wicks, "nBn detector, an infrared detector with reduced dark current and higher operating temperature," *Appl. Phys. Lett.*, vol. 89, no. 15, 2006, Art. no. 151109. [Online]. Available: <https://doi.org/10.1063/1.2360235>
- [5] S. Maimon, "Reduced dark current photodetector," U.S. Patent 7 687 871 B2, Mar. 30, 2010.
- [6] P. Klipstein, "Depletion-less photodiode with suppressed dark current and method for producing the same," U.S. Patent 7 795 640 B2, Sep 14, 2010.
- [7] P. Klipstein, "XBN barrier photodetectors for high sensitivity and high operating temperature infrared sensors," *Proc. SPIE*, vol. 6940, 2008, Art. no. 69402U. [Online]. Available: <https://doi.org/10.1117/12.778848>
- [8] B. M. Nguyen, G. Chen, A. M. Hoang, S. Abdollahi Pour, S. Bogdanov, and M. Razeghi, "Effect of contact doping in superlattice-based minority carrier unipolar detectors," *Appl. Phys. Lett.*, vol. 99, 2011, Art. no. 033501. [Online]. Available: <https://doi.org/10.1063/1.3613927>
- [9] D. Z.-Y. Ting *et al.*, "A high-performance long wavelength superlattice complementary barrier infrared detector," *Appl. Phys. Lett.*, vol. 95, 2009, Art. no. 023508. [Online]. Available: <https://doi.org/10.1063/1.3177333>
- [10] D. Z.-Y. Ting *et al.*, "Exclusion, extraction, and junction placement effects in the complementary barrier infrared detector," *Appl. Phys. Lett.*, vol. 102, no. 12, 2013, Art. no. 121109. [Online]. Available: <https://doi.org/10.1063/1.4798551>
- [11] J. R. Pedrazzani, S. Maimon, and G. W. Wicks, "Use of nBn structures to suppress surface leakage currents in unpassivated InAs infrared photodetectors," *Electron. Lett.*, vol. 44, no. 25, pp. 1487–1488, 2008. doi: [10.1049/el:20082925](https://doi.org/10.1049/el:20082925).
- [12] G. R. Savich, J. R. Pedrazzani, S. Maimon, and G. W. Wicks, "Suppression of surface leakage currents using molecular beam epitaxy-grown unipolar barriers," *J. Vac. Sci. Technol. B*, vol. 28, 2010, Art. no. C3H18. [Online]. Available: <https://doi.org/10.1116/1.3276513>
- [13] L. Bürkle and F. Fuchs, "InAs/(GaIn)Sb superlattices: A promising material system for infrared detection," in *Handbook of Infrared Detection Technologies*, M. Henini and M. Razeghi, Ed. Oxford, U. K.: Elsevier Science, 2002, pp. 159–189.
- [14] M. Razeghi and F. Mohseni, "GaSb/InAs superlattices for infrared FPAs" in *Handbook of Infrared Detection Technologies*, M. Henini and M. Razeghi, Ed. Oxford, U. K.: Elsevier Science, 2002, pp. 191–232.
- [15] D. Z.-Y. Ting *et al.*, "Type-II superlattice infrared detectors" in *Semiconductors and Semimetals*, vol. 82, *Advances in Infrared Photodetectors*, S. Gunapala, D. Rhiger, and C. Jagadish, Ed. New York, NY, USA: Elsevier–Academic, 2011, pp. 1–57.
- [16] D. Donetsky, S. P. Svensson, L. E. Vorobjev, and G. Belenky, "Carrier lifetime measurements in short-period InAs/GaSb strained-layer superlattice structures," *Appl. Phys. Lett.*, vol. 95, 2009, Art. no. 212104. doi: [10.1063/1.3267103](https://doi.org/10.1063/1.3267103).
- [17] E. H. Steenberg *et al.*, "Significantly improved minority carrier lifetime observed in a long-wavelength infrared III-V type-II superlattice comprised of InAs/InAsSb," *Appl. Phys. Lett.*, vol. 99, 2011, Art. no. 251110. [Online]. Available: <https://doi.org/10.1063/1.3671398>
- [18] B. V. Olson *et al.*, "Time-resolved optical measurements of minority carrier recombination in a mid-wave infrared InAsSb alloy and InAs/InAsSb superlattice," *Appl. Phys. Lett.*, vol. 101, 2012, Art. no. 092109. [Online]. Available: <https://doi.org/10.1063/1.4749842>
- [19] L. Höglund *et al.*, "Influence of radiative and non-radiative recombination on the minority carrier lifetime in midwave infrared InAs/InAsSb superlattices," *Appl. Phys. Lett.*, vol. 103, 2013, Art. no. 221908. doi: [10.1063/1.4835055](https://doi.org/10.1063/1.4835055).
- [20] D. Z. Ting, A. Khoshakhlagh, A. Soibel, C. J. Hill, and S. D. Gunapala, "Barrier infrared detector," U. S. Patent 8 217 480, Jun. 14, 2012.
- [21] P. C. Klipstein *et al.*, "Modeling InAs/GaSb and InAs/InAsSb superlattice infrared detectors," *J. Electron. Mater.*, vol. 43, pp. 2984–2990, 2014. [Online]. Available: <https://doi.org/10.1007/s1166>
- [22] I. Vurgaftman *et al.*, "Interband absorption strength in long-wave infrared type-II superlattices with small and large superlattice periods compared to bulk materials," *Appl. Phys. Lett.*, vol. 108, 2016, Art. no. 222101.
- [23] D. Z. Ting, A. Soibel, and S. D. Gunapala, "Hole effective masses and subband splitting in type-II superlattice infrared detectors," *Appl. Phys. Lett.*, vol. 108, 2016, Art. no. 183504. [Online]. Available: <https://doi.org/10.1063/1.4948387>
- [24] D. Z. Ting, A. Soibel, and S. D. Gunapala, "Type-II superlattice hole effective masses," *Infrared Phys. Technol.*, vol. 84, pp. 102–106, 2017. [Online]. Available: <https://doi.org/10.1016/j.infrared.2016.10.014>
- [25] D. Z. Ting *et al.*, "Mid-wavelength high operating temperature barrier infrared detector and focal plane array," *Appl. Phys. Lett.*, vol. 113, 2018, Art. no. 021101. doi: [10.1063/1.5033338](https://doi.org/10.1063/1.5033338).
- [26] W. E. Tennant, "Rule 07 Revisited: Still a good heuristic predictor of p/n HgCdTe photodiode performance?," *J. Electron. Mater.*, vol. 39, no. 7, pp. 1030–1035, 2010. [Online]. Available: <https://doi.org/10.1007/s11664-010-1084-9>